

Alma Mater Studiorum Università di Bologna  
Archivio istituzionale della ricerca

Boc-Protection on L-DOPA: an Easy Way to Promote Underwater Adhesion

This is the final peer-reviewed author's accepted manuscript (postprint) of the following publication:

*Published Version:*

Giuri, D., Jacob, K.A., Ravarino, P., Tomasini, C. (2020). Boc-Protection on L-DOPA: an Easy Way to Promote Underwater Adhesion. EUROPEAN JOURNAL OF ORGANIC CHEMISTRY, 2020(46), 7144-7150 [10.1002/ejoc.202001264].

*Availability:*

This version is available at: <https://hdl.handle.net/11585/804581> since: 2021-02-23

*Published:*

DOI: <http://doi.org/10.1002/ejoc.202001264>

*Terms of use:*

Some rights reserved. The terms and conditions for the reuse of this version of the manuscript are specified in the publishing policy. For all terms of use and more information see the publisher's website.

This item was downloaded from IRIS Università di Bologna (<https://cris.unibo.it/>).  
When citing, please refer to the published version.

(Article begins on next page)

This is the final peer-reviewed accepted manuscript of:

Giuri, D.; Jacob, K. A.; Ravarino, P.; Tomasini, C. Boc-Protection on L-DOPA: An Easy Way to Promote Underwater Adhesion. *European Journal of Organic Chemistry* **2020**, 2020 (46), 7144–7150.

The final published version is available online at:  
<https://doi.org/10.1002/ejoc.202001264>

#### Terms of use:

Some rights reserved. The terms and conditions for the reuse of this version of the manuscript are specified in the publishing policy. For all terms of use and more information see the publisher's website.

This item was downloaded from IRIS Università di Bologna (<https://cris.unibo.it/>)

**When citing, please refer to the published version.**

## REVIEW

# L-Dopa in Small Peptides: An Amazing Functionality to Form Supramolecular Materials

Demetra Giuri,<sup>a</sup> Paolo Ravarino<sup>a</sup> and Claudia Tomasini<sup>a\*</sup>

Received 00th January 20xx,  
Accepted 00th January 20xx

DOI: 10.1039/x0xx00000x

L-Dopa (3,4-dihydroxyphenylalanine) is a chiral amino acid generated via biosynthesis from L-tyrosine in plants and some animals. The presence of multiple interacting sites makes L-Dopa a multifunctional building block for the preparation of supramolecular materials. The possibility to form hydrogen bonds and the presence of the aromatic ring allow L-Dopa molecules to interact through a series of non-covalent interactions. The additional presence of the catechol moiety really makes this compound unique: not only it has implications in the self-assembly process of Dopa itself and with other substrates, but also highly increases the number of applications of the final material, since it works as antioxidant, radical trapper, metal chelator, reducing agent and adhesive. L-Dopa and catechol containing derivatives have been extensively introduced inside both synthetic and natural polymers to obtain amazing functional materials. In this review we report the preparation of small peptides containing L-Dopa, focusing on the supramolecular materials that can be obtained with them, ranging from fibrils to fibres, gels, films and coatings, all having the different applications mentioned above and many others.

## Introduction

L-Dopa (3,4-dihydroxyphenylalanine, abbreviated as Z) is a chiral amino acid that is involved in several biosynthetic pathways. It is a multifunctional building block that leads to the preparation of various materials. Before describing the formation of supramolecular materials obtained with this amino acid, we introduce here its preparation and its properties.

The biosynthesis of L-Dopa takes place in several organisms, spanning from plants to animals, mushrooms and bacteria. It involves tyrosinase, a copper-dependent enzyme, that shows two distinct activities, both involving molecular oxygen: cresolase (or monophenolase) and catecholase (or diphenolase). The first one is the responsible for the *ortho*-hydroxylation of tyrosine, leading to the formation of Dopa, while the second one oxidises *o*-diphenols to *o*-quinones (Figure 1).<sup>1</sup>

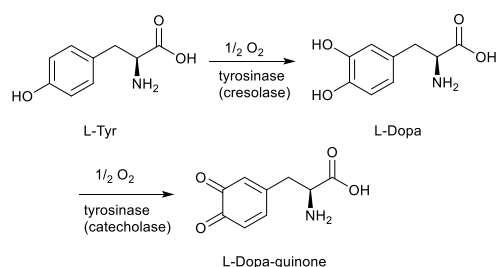


**Figure 1.** Tyrosinase activity to convert L-Tyr in L-Dopa and L-Dopa-quinone.

Mushroom tyrosinase is a widely used enzyme also for a synthetic approach, due to its commercial availability and remarkable

solubility.<sup>2</sup> As the major product is the oxidised form *o*-quinone, a reduction to afford Dopa is required, using ascorbic acid or NADH as reductant. Moreover, Min *et al.* reported an example of electroenzymatic reaction that reduces *in situ* the Dopa quinone using a tyrosinase-immobilised cathode under the reduction potential of L-Dopa (-530mV).<sup>3</sup> The high conversion rate obtained (95.9%), coupled to the ease of separation from the media, makes this methodology an interesting way to produce L-Dopa.

L-Dopa may be also obtained by chemical synthesis. This compound was first prepared by Waser and Lewandowski, through the use of a chiral pool.<sup>4</sup> Later on, several example of synthetic preparations that involve the asymmetric catalysis were described.<sup>5–8</sup> These processes are often very long, use expansive catalysts or afford modest yields. Based on a previous study on the phenols oxidation,<sup>9</sup> another synthetical approach mimicking the activity of mushroom tyrosinase has been reported by Bernini *et al.*<sup>10</sup> and involves the use of normal reagents instead of a catalytic driven process. They reported a one-pot synthesis of L-Dopa starting from L-Tyr and using 2-iodoxybenzoic acid (IBX) in small excess for the oxidation. This first step leads to the formation of the *o*-quinone, mimicking the activity of the enzyme, then an *in situ* reduction is carried out with sodium dithionite to afford L-Dopa (Figure 2). It is worth noticing that this process has high yield (95%) and leaves the chiral centre unaltered.

<sup>a</sup> Dipartimento di Chimica Giacomo Ciamician – Università di Bologna – Via Selmi, 2 – 40126 Bologna - Italy

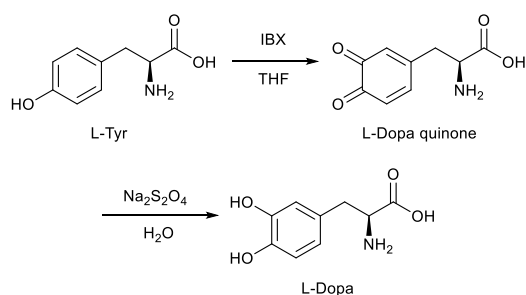


**Figure 2.** L-Dopa synthetic path followed by Bernini's group.

L-Dopa is a crucial intermediate for the biosynthesis of several compounds: its oxidative polymerisation produces melanin and can be mimicked to prepare biomaterials such as eumelanin and pheomelanin.<sup>11</sup>

Moreover, L-Dopa is the precursor of dopamine, epinephrine and norepinephrine, which are neurotransmitters that play important roles in controlling health and well-being (Figure 3). Dopamine plays a central role in the treatment of Parkinson's disease, but is yet unable to pass the blood brain barrier (BBB). L-Dopa is used to increase dopamine levels in blood as it can pass the BBB.

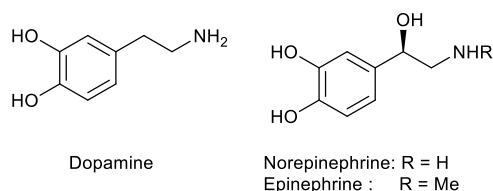


**Figure 3.** Chemical structure of catecholamines.

L-Dopa is present in naturally occurring polymers mainly synthesised by marine organisms,<sup>12</sup> such as the *Mytilus edulis* (blue mussels) able to secrete the byssus.<sup>13,14</sup> Mussels use the byssus, a protein-based adhesive, for securing themselves to various underwater surfaces, such as sea rocks and ship hulls, and resist detachments even in marine's harsh and wavy conditions.<sup>15,16</sup> The byssus consists of a bundle of threads composed by three parts: the adhesive plaque, the rigid distal thread and the flexible proximal thread. The byssal thread is composed by the mussel foot, which is the flexible part responsible for the adhesion on the target surface. So far, roughly 25-30 different mussel foot proteins (mfps) have been identified in byssus, 5 of them (mfp-2 to mfp-6) being unique to the plaque.<sup>14,15,17</sup> Mfp-3 and mfp-5 are considered the main responsible for the adhesion of the plaque to the surface and contain a particularly high amount (up to 30 mol%) of L-Dopa.<sup>18</sup> For this reason, it is widely believed that L-Dopa, and in particular its catechol group, have a dominant role in wet binding.<sup>19</sup> So far, several excellent reviews have been written on mussel-inspired polymers: hydrogels for biomedical<sup>20-22</sup> and environmental<sup>23</sup> applications, adhesives,<sup>24,25</sup> antifouling coatings.<sup>26</sup> Many of them carefully describe the chemistry of the catechol group, the principles of wet adhesion with L-Dopa derivatives and the effect of the oxidation, how to prepare polymers containing L-Dopa, dopamine or catechol moieties.<sup>20,21,25</sup> About the last topic, a number of strategies has been used to modify both natural and synthetic polymers, in order to insert Dopa or catechol motifs along the chain

or laterally grafted. The polymerization of catechol-modified monomers has been widely reported, with starting monomers such as dopamine-methacrylamide, catechol-containing vinyl groups, catechol-containing epoxide, which is then possible to copolymerise with other polymers obtaining several other materials.

The direct functionalization of polymers with Dopa and dopamine can be obtained via the formation of amide, urethane and ester linkages with the functional groups –NH<sub>2</sub>, –COOH and –OH. It was reported for both synthetic polymers and copolymers (PEG, poly(ethylene) oxide, polycaprolactone) and biopolymers (gelatine, chitosan, dextran, hyaluronic acid, alginate).<sup>21</sup>

Wet adhesives of reduced complexity consist of low-molecular-weight catecholic zwitterionic surfactants, as mussels foot proteins (Mfps), that are polyelectrolytes with high charge density.<sup>27</sup>

L-Dopa-containing polypeptides have been prepared to mimic Mfps, usually through solid-phase peptide synthesis method, and then cross-linked with tyrosinase.<sup>21</sup>

Wound sealants may attach to tissues by molecular cross-linking or through mechanical interlocking with the underlying tissue. Three types of wound sealants can be prepared: biopolymers, synthetic polymers or biosynthetic composites. Among them we can find:

- mussel-derived sealants, where L-Dopa catechol is readily oxidised, leading to intermolecular crosslinking and quick formation of water-resistant bonds with the substrate;
- biologically inspired sealants, such as branched and linear synthetic polymers containing Dopa;
- polypeptide analogues of MAPs containing Dopa and L-Lys obtained through ring-opening metathesis polymerization (ROMP).<sup>28</sup>

Although it is widely believed that wound sealants will replace sutures, application of adhesive hydrogels as wound sealant is still limited. Synthetical materials tend to act as physical barriers, probably because of their lack of bioactivity for blood coagulation and wound healing. Solid materials require manual pressure to heal a bleeding site. Liquid materials usually require some preparation and are mainly for minor or mild haemorrhage. Fibrin-based sealants are the most effective, but they are the most expensive and the risk of viral infections is not negligible. Chitosan is widely used as haemostatic biomaterial. Other biopolymer-based materials are used, but no one is really effective for stopping severe bleeding.<sup>28</sup>

## Supramolecular Materials Obtained with Short Peptides Containing L-Dopa

Molecular assembly is a ubiquitous process in nature. Peptides and proteins, for example, interact and self-organize to form well-defined structures associated with specific functionalities. Mimicking nature, we can exploit self-assembly for the preparation of an entirely novel class of synthetic materials.

The self-assembly of small molecules relies on weak non-covalent interactions, such as hydrogen bonds, electrostatic interactions, hydrophobic interactions and van der Waals interactions.<sup>29,30</sup> Although very weak if isolated, these interactions gain significant importance when combined as a whole and are able to govern the

formation of complex structures.<sup>31</sup>

Since one usual consequence of the self-assembly of small molecules, and in particular of peptides, is the formation of a gel (gelation), a subset of these compounds is that of low molecular weight gelators (LMWGs), which gained increasing relevance in the last two decades.

Compared to their polymeric analogues, in which the random network is held together by strong covalent interactions and cross-linking, LMWGs rely on weak bonds and molecular assembly, thus making the process not only more ordered but also reversible.

It is possible to trigger the formation of the material in specific conditions and, in the same way, to induce the disassembly of the network if the condition is reversed. For their ability to respond to external stimuli, LMWGs are considered a class of smart materials.

The sol-gel transition is usually induced by a stimulus (trigger), that can be physical (a temperature change, ultrasound, ionic strength modulation) or chemical (pH change, chemical or photochemical reactions, enzymes and catalysis).<sup>32</sup> The general method of preparation relies first on the dissolution of the gelator molecule into a solvent (water for hydrogels, organic solvent for organogels), followed by the addition of the trigger to the solution. This leads to the start of the assembly process, inducing the molecules to organise into supramolecular structures, which are usually fibres, that entangle together over time, resulting in a network able to entrap the solvent.

This class of soft materials results particularly interesting for several reasons, first of all the possibility to easily tune and control the chemical structure of the gelator and the conditions of the gelation process, thus changing the specific properties and applications of the final material. Moreover, LMWGs derived from amino acids and peptides result even more appealing thanks to their intrinsic biocompatibility and biological activity.<sup>33</sup>

L-Dopa is an ideal ligand for several substrates. The two hydroxyl groups create hydrogen bonds and their *ortho*-position makes L-Dopa a strong chelating agent, while the aromatic feature creates  $\pi$ - $\pi$  stacking, cation- $\pi$  and van der Waals interactions. Nevertheless, the oxidised form, Dopa-quinone, is worth of notice: the two carbonyl groups can act as Lewis bases, even though weaker than the deprotonated catecholic form. The conjugated system of four double bonds enables the molecule to absorb and emit visible light. The quinone is also able to hydrogen bond with the catechol (Figure 4). The formation of these weak interactions is of remarkable importance when considering the preparation of a L-Dopa-based material: the cohesion strength is enhanced and so the rheological properties.

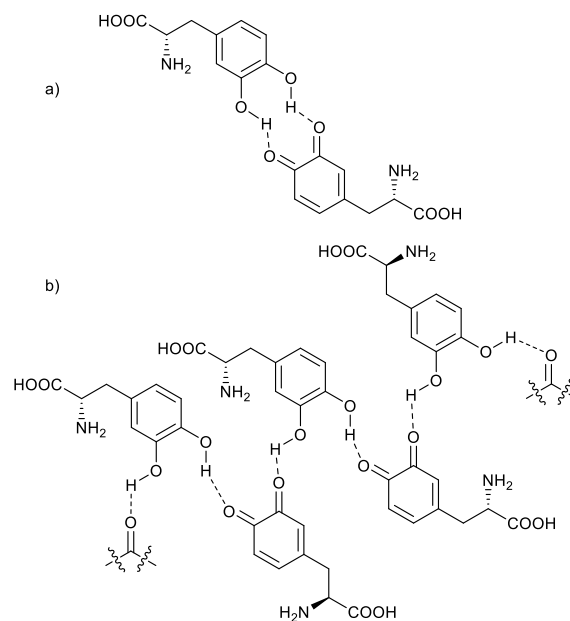


**Figure 4.** Intermolecular hydrogen bonds between L-Dopa molecules in the reduced and oxidised forms: **a)** bimolecular hydrogen bonds, **b)** oligo- or polymolecular hydrogen bonds.

We believe that the possibility to exploit Dopa and its functionalities as building block in supramolecular assembly is worth reporting, since it leads to the preparation of amazing materials, with a wide range of architectures, properties, morphologies and applications.

The aim of our review is to fill this gap, with a journey through the small peptides based on L-Dopa, from single amino acids (like Fmoc-L-Dopa) to dipeptides and so on, slowly increasing the chain length. We will report the self-assembled structures and the universe of applications that can be achieved using this simple building block.

We will present an overview of the materials that can be obtained, focusing on the formation techniques required to promote their self-assembly and on the properties of the material. For a better understanding, the examples will be organized, showing the materials that are formed by single protected L-Dopa, then by L-Dopa containing dipeptides, tripeptides, and so on till the use of hexapeptides. Finally, some examples of mfps analogues, containing up to 25 amino acids, will be reported.

#### Protected L-Dopa: a Single Amino Acid Gelator

Saha *et al.* were the first group to report a self-assembly study on a single amino acid gelator based on L-Dopa. The behaviour of Fmoc-L-Dopa solutions (0.5% wt) in water was investigated at different pH conditions: pH = 2, 5, 7.<sup>34</sup> Only at pH 2 it was possible to obtain a mechanically weak gel, while increasing the pH no gel was formed and the solutions turned brown in colour with time, due to the oxidation of the catechol moiety. The characterisation of the solutions (CD, DLS, SAXS, TEM and cryo-TEM) allowed them to predict a schematic model for the self-assembly of Fmoc-L-Dopa at pH 2 (Figure 5).

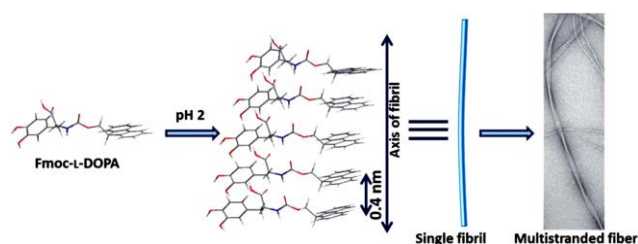


**Figure 5.** Schematic representation for the proposed model of self-assembly of Fmoc-L-Dopa at pH 2. Adapted with permission from ref. 34. Copyright (2013) Royal Society of Chemistry.

They proposed that monomers stack linearly along the axis of the fibril, stabilized via  $\pi$ - $\pi$  interactions among the Fmoc groups. The possibility of intermolecular H-bonding between the C=O and N-H of the adjacent carbamate groups was also proposed. At higher pH conditions (pH 5 and 7) the majority of Fmoc-L-Dopa molecules were ionized due to deprotonation of the carboxylic group and this resulted in inhibition of fibril formation.

The assembly of Fmoc-L-Dopa (1 mg/mL) was also investigated in ethanol/water mixed solutions.<sup>35</sup> This solvent change method consists in the dissolution of the gelator in an organic solvent and the following addition of a miscible anti-solvent, such as water, which reduces the solubility of the compound and induces the gelation process. Gazit *et al.* reported that, despite its apparent simplicity, under these conditions Fmoc-L-Dopa participates in complex, spontaneous structural transitions with intermediate metastable assemblies. Upon the initiation of assembly, Fmoc-L-Dopa rearranges into metastable spheres, which are in continuous equilibrium with the dissolved monomers. The monomers serve as a reservoir for the formation of supramolecular assembly in the gel phase, mainly mediated by hydrophobic interactions. The disordered aspects of the spheres and the fibrillar assemblies are a kinetically driven product that arises from dynamic competition and interaction with solvent molecules. The conclusion of the transition process resulted in the formation of crystals, 1 month after the start of the process. A network of hydrogen bonds between Dopa moieties leads to the locking of Fmoc-Dopa molecules in a thermodynamically favourable ultrastructure. As reported in other works, the molecular packing of the gel phase is different from that observed in the crystal phase.<sup>36</sup> Fmoc-Dopa system is considered a minimal multiphase model for supramolecular polymers in which diverse molecular forces participate at the different stages of structural transitions (Figure 6).

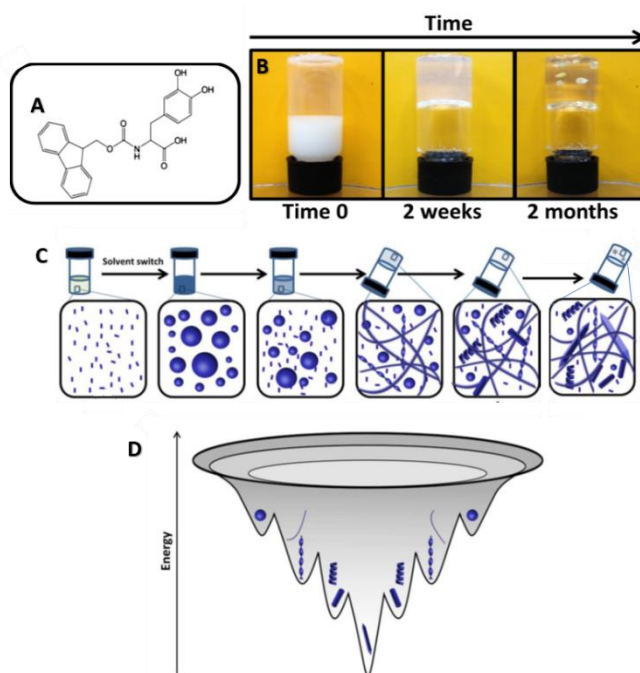


**Figure 6.** (A) Chemical structure of Fmoc-L-Dopa. (B) Macroscopically observable changes of Fmoc-Dopa preparation over time. (C) Suggested model for the Fmoc-Dopa structural transition process. Schematic diagram showing a sol-gel-crystal transition that occurs at the macroscopic level, with an underlying morphological transition at the microscopic level. (D) Energy landscape of the Fmoc-Dopa transition process.

Later on, Gazit *et al.* investigated the behaviour of Fmoc-Dopa in a mixture of DMSO and water and in combination with Fmoc-Tyr.<sup>37</sup> In their work they demonstrated how the functionalities of Dopa can be exploited in multicomponent gels and are crucial to provide specific properties and achieve materials with interesting applications. When prepared from DMSO/water solutions (5 and 6.67 mg/mL), Fmoc-Dopa preparations were viscous and presented a weak, non-self-supporting gel-like behaviour, while Fmoc-Tyr hydrogels exhibited self-supporting gel characteristics within minutes after triggering.

The mixed system combined the properties of the two components, joining the physical characteristics of Fmoc-Tyr gels and the functionality of the catechol groups of Dopa. The ability of the multicomponent hydrogel to reduce ionic silver to Ag nanoparticles (AgNP) was investigated. Silver nitrate solution was added to fully formed hydrogels which were then incubated in the presence or absence of ambient light for five days. AgNP were detected in the Fmoc-Dopa and hybrid gel samples, as imaged by TEM (Figure 7) and attributed to the catechol functionality and the presence of light.

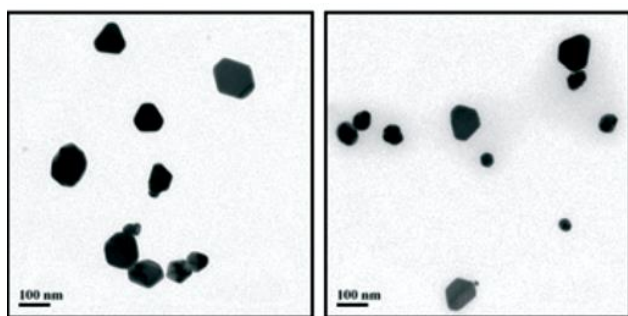


**Figure 7.** TEM micrographs of silver nanoparticles detected in samples of 1.67 mg mL<sup>-1</sup> Fmoc-Dopa (left panel) and Fmoc-Tyr:Fmoc-Dopa 3 : 1 hybrid gels at 6.67 mg mL<sup>-1</sup> (right panel), following incubation with silver nitrate in the presence of light. Adapted with permission from ref. 37. Copyright (2015) Royal Society of Chemistry.

An efficient way to obtain strong hydrogels ( $G' = 25\text{--}64$  KPa depending on the trigger) with a single amino acid gelator based on L-Dopa was recently reported by Tomasini *et al.*, with the synthesis of Boc-L-Dopa(Bn)<sub>2</sub>-OH,<sup>38</sup> that is a Dopa derivative where the benzyl ethers linked to the catechol moiety proved to be essential for the formation of strong supramolecular gels, thanks to the additional  $\pi$ - $\pi$  stacking interactions provided. The gels were prepared using two methods: pH change, using glucono- $\delta$ -lactone (GdL) as trigger, and addition of CaCl<sub>2</sub>, a divalent cation. The two methods led to the formation of materials with different mechanical properties, morphologies and structures. The gels prepared with CaCl<sub>2</sub> were used for the controlled growth of CaCO<sub>3</sub> crystals. The reported soft biomaterial represents a model for biomineralization studies where the hydrogel structure can act as an analogue of the insoluble matrix

that confines the calcification site, provides Ca<sup>2+</sup>, and preserves its structure (Figure 8) after the formation of the mineral phase.

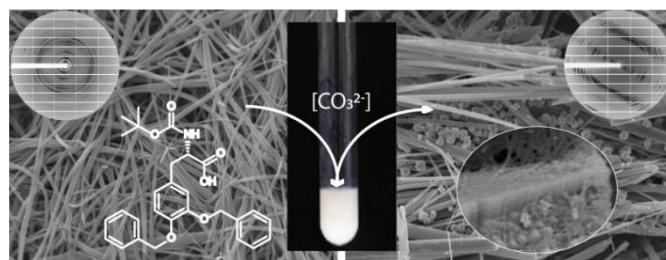


**Figure 8.** Schematic depiction of the formation of Boc-L-Dopa(Bn)<sub>2</sub>-OH hydrogels using two triggers, GdL and CaCl<sub>2</sub>. Adapted with permission from ref. 38. Copyright (2019) American Chemical Society.

Lee *et al.* reported the preparation of Dopa-C7 bolaamphiphile, composed of a central heptyl chain and two Dopa moieties at the ends (Figure 9).<sup>39</sup> The self-assembly of the compound was used as template to produce magnetic metal oxide core-shell nanoparticles. The catechol group adsorbs metal cations through chelation with hydroxyl and quinone moieties. Taking advantage of this metal ion adsorption, cobalt and iron ions were bound and subsequently reduced to create solid metal oxides on the Dopa-C7 self-assembly template. As for many organic substances, the Dopa-C7 self-assembly did not show noticeable magnetic susceptibility to an external magnetic field. After deposition of a cobalt oxide or iron oxide layer, the core-shell particle displayed paramagnetic behaviour showing linear magnetization over the external magnetic field with negligible coercivity and magnetic remanence. Cobalt oxide showed stronger magnetization than iron oxide.



**Figure 9.** Schematic layout of the Dopa-C7 self-assembly and subsequent metal ion adsorption for the synthesis of magnetic cobalt and iron oxide nanoparticles.

The self-assembly of this compound is robust and stable even under vacuum and in dry conditions, with adhesive properties arising from the surface-exposed catechols. The authors observed that, when Dopa-C7 molecules are dissolved in aqueous solutions, they spontaneously self-assemble, creating nanospherical aggregates with exposed Dopa catechol moieties on the surface, which over time also aggregate forming bigger structures. These clusters then assemble through the hydrogen bond working between the

dihydroxyphenyl groups to form spherical assembled structures ( $87.5 \pm 9.1$  nm in diameter).

This suspension was applied as an adhesive to modify the surfaces of various substrates. Dopa-C7 assemblies were stamped on a silicon wafer, leading to the formation of a coating on the surface (Figure 10), with homogeneity higher than that of polydopamine.

Dopa-C7 assemblies also showed considerable adhesivity, originated from the hydrogen bonding of catechol groups, remarkable enhanced cell adhesion, increased cell viability and lower toxicity compared to the other catechol-modified surfaces.



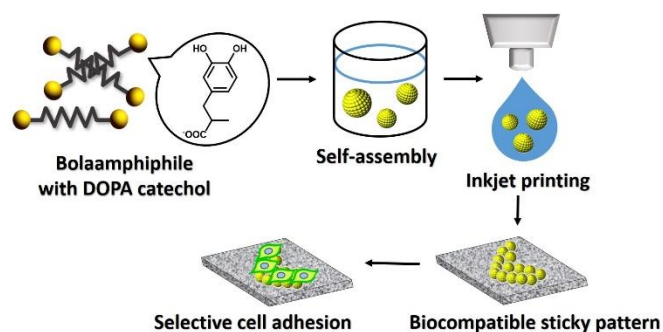


**Figure 10.** Schematic illustration of the selective cell adhesion on a patterned surface that was prepared by the inkjet printing of bolaamphiphile assemblies.

Tomasini *et al.* recently described a new class of Dopa-based adhesives that consists in extremely simple molecules,<sup>40</sup> where the catechol moiety is partly or fully protected with Boc groups.

Three molecules were synthesised to probe how the introduction of hydrophobic groups would affect the adhesive ability of the Dopa skeleton: Boc-L-Dopa-OMe, an inseparable mixture of *m*-Boc<sub>2</sub>-L-Dopa-OMe and *p*-Boc<sub>2</sub>-L-Dopa-OMe, and Boc<sub>3</sub>-L-Dopa-OMe.

Three films were prepared by casting the molecules on a petri dish. After solvent evaporation, the films resulted completely non-adhesive in the dry phase, while the adhesion was triggered after wetting with three aqueous media (H<sub>2</sub>O, 1M aqueous CaCl<sub>2</sub> and PBS at pH 7.4). In contrast, Boc-L-Dopa-OMe showed no adhesion capability neither in dry nor in wet conditions.

The inseparable mixture of *m*-Boc<sub>2</sub>-L-Dopa-OMe and *p*-Boc<sub>2</sub>-L-Dopa-OMe registered an adhesive force up to 130 N in 1M aqueous CaCl<sub>2</sub> (Figure 11). In contrast, the adhesion registered with Boc<sub>3</sub>-L-Dopa-OMe showed the best performances in the other aqueous solutions suggesting that, even though the protection on the catechol prohibits the cations chelation, it allows a fast dehydration of the surface to bind.

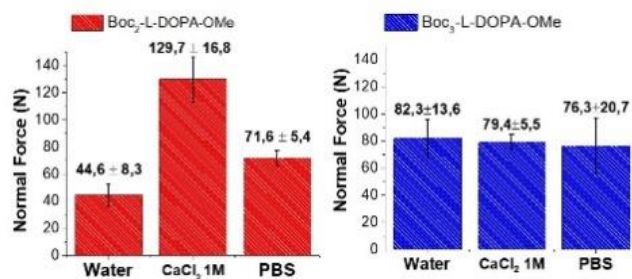


**Figure 11.** Results for the traction tests of Boc<sub>2</sub>-L-Dopa-OMe and Boc<sub>3</sub>-L-Dopa-OMe

#### Self-assembled L-Dopa Containing Di- and Tri-Peptides

After the first group of molecules containing a single L-Dopa unit, we report here the preparation of supramolecular materials based on longer peptides containing L-Dopa.

Tomasini *et al.* reported the gelation ability of Fmoc-L-Dopa-D-Oxd-OH, Fmoc-L-Tyr-D-Oxd-OH and Fmoc-L-Phe-D-Oxd-OH in water using several gelators (Figure 12).<sup>41</sup>

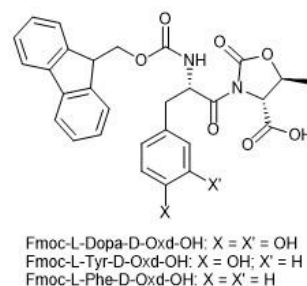


**Figure 12.** Chemical structure of the gelators described.

They introduced the 4-methyl-5-carboxyoxazolidin-2-one (Oxd) moiety that is a derivative of threonine. This heterocycle introduces a constraint imposed by the *trans* conformation of the two adjacent carbonyls, that can favour the formation of fibre-like materials organized either in  $\beta$ -sheets or in supramolecular helices when combined with other factors, like  $\pi$ -stacking interactions and intermolecular hydrogen bonds.<sup>42</sup> Indeed, when Oxd was replaced with Pro, only liquids or amorphous solids were obtained.

Supramolecular gels were prepared using these three gelators and ten different triggers. The results indicated that hydrogel formation was very sensitive to both the number of the hydroxyl moieties linked to the aromatic rings and the nature of the trigger. The best triggers for these systems were GdL, CaCl<sub>2</sub> and ZnCl<sub>2</sub> leading to hydrogels with mechanical properties depending on the gelator used. Fmoc-L-Tyr-D-Oxd-OH resulted the strongest in all cases.

In a following work, Tomasini *et al.* reported a comparison between the gelation ability of Fmoc-L-Dopa(Bn)<sub>2</sub>-D-Oxd-OBn and Lau-L-Dopa(Bn)<sub>2</sub>-D-Oxd-OBn in several organic solvents using ultrasound sonication as trigger. The first gelator was not able to form gels in any of the solvents.<sup>43</sup> The second one formed gels in toluene, ethyl acetate, acetonitrile, ethanol and methanol, suggesting that the presence of the saturated long chain of lauric acid was essential for its tendency to stick together producing fibres and micelles. The mechanical properties and melting point of the materials were found to be directly correlated to the polarity of the solvent, resulting in increasing strength moving from toluene to ethanol. The ethanol organogel was used to test the absorption of Rhodamine B as a model pollutant from water. After 24 h, only the 23% of the pollutant remained in the aqueous solution (Figure 13).

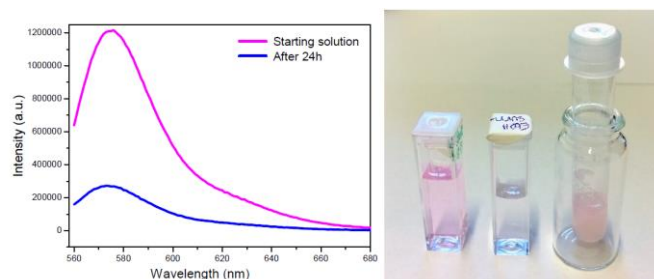


**Figure 13.** (Left) Emission spectra of an aqueous solution of RhB (2.0  $\mu$ M) (pink) and of the same solution after being treated with the ethanol organogel for 24 hours (blue). (Right) Photograph of a fresh sample of the aqueous solution of RhB, of the same sample after treatment with the ethanol organogel, and of the organogel after 24 h (from left to right).



Gazit *et al.* reported that L-Dopa-L-Dopa and Fmoc-L-Dopa-L-Dopa dipeptides were able to self-assemble into ordered nanostructures in the presence of ethanol and water.<sup>44</sup>

They observed the temperature dependent formation of a gel for Fmoc-L-Dopa-L-Dopa (Figure 14).

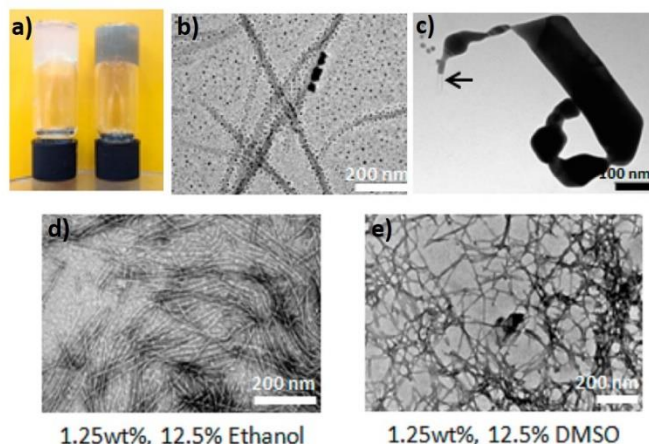


**Figure 14.** Top: a) Macroscopic visualization of assemblies at 5 mg/mL taken after 5 days of incubation. b) TEM micrographs of the formation of silver particles after 1 day of incubation of assemblies at 2.5 mg/mL. c) TEM micrographs of the assemblies at 5 mg/mL after 3 days of incubation. The arrows indicate noncoated peptide assemblies (negative staining was not applied). Bottom: TEM analysis of 1.25 wt % (17.2 mM) Fmoc-Dopa-Dopa-Lys assemblies prepared in either 12.5% ethanol (d) or 12.5% DMSO (e).

The authors investigated the redox properties of the assemblies containing the catechol moieties by monitoring the reduction of ionic silver. Although these assemblies were found to possess redox activity due to their decoration with catechol functional groups, no adhesive properties were macroscopically observable. Therefore, they designed the Fmoc-L-Dopa-L-Dopa-L-Lys protected tripeptide, inspired by mussel foot proteins (mfps), that base their adhesive strength on the synergy between Dopa and Lys.

Under both ethanol and DMSO conditions, they observed that this tripeptide forms viscoelastic glue capable of adhering two glass slides. In the presence of DMSO, the adhesive properties (more than 300 nN with AFM) showed recovery behaviour: after separating the glass slides by peeling, they were able to be rejoined, and the AFM analysis revealed the presence of twisted spheres that were unidirectionally retracted. Interestingly, this did not happen in ethanol, where the adhesive force was also a bit lower (214 nN) and AFM analysis after peeling exhibited unidirectional fine fibrous structures. The authors therefore hypothesised that the existence of the larger patches of peptide assemblies have a role in the re-adhesion process.

### 2.3. Self-assembled Dopa Tetra- and Pentapeptides

Materials obtained by the self-assembly of peptides containing 4 or 5 amino acid show interesting properties. In several examples described here, the property is exploited by only one Dopa unit.

Xu *et al.* reported the preparation of a bioadhesive supramolecular hydrogel containing Dopa (Fmoc-Leu-Phe-Phe-Dopa) via protease catalysis (Figure 15).

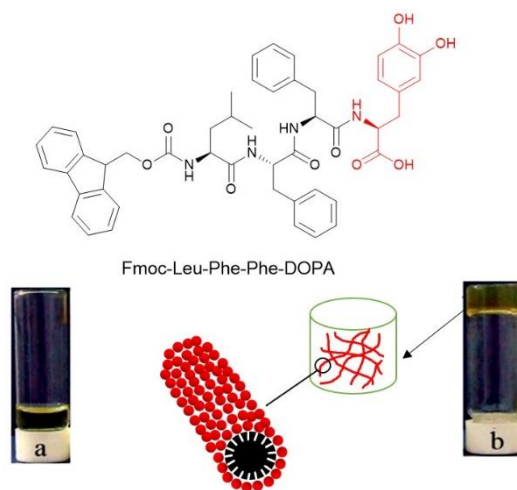


**Figure 15.** Chemical structures of the (NPC 15199 + Phe-Phe-Dopa) and enzymatic formation of the hydrogelator (Fmoc-Leu-Ohe-Phe-Dopa); a) solution containing 40 mM 1 and 2 with inactive metalloprotease, pH 7.4; b) gel formed with the catalysis of metalloprotease after 5 min.

The authors observed that catechol groups are important for tuning the balance between the hydrophilicity and the hydrophobicity of the resulting gelators, which will affect their gelation behaviour. Dopa's ability to promote cell adhesion and proliferation, respectively, using *in vitro* cellular experiments was evaluated. A hydrogel based on Fmoc-Lys-Phe-Phe without Dopa was used as control. Adult human dermal fibroblast cells were seeded on top of the gels. The results showed that more cells adhered to the Dopa-containing gel, and cell viability (Figure 16) at day 3 was 152% greater than day 1 (35% more than the control). This result demonstrated that the effective presence of the unoxidized catechol groups successfully promoted the adhesion and proliferation of fibroblast cells relative to the gels without Dopa.

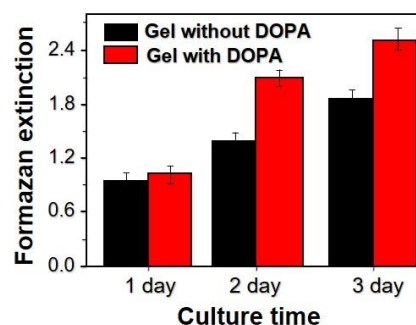


**Figure 16.** Proliferation rate of cells on gels containing DOPA groups and the control (without DOPA) determined using the WST-8 method.

The peptide described by Ying *et al.* is prepared through a different approach, by *in situ* enzymatic formation of Dopa hydrogels (5 mg/mL), using a simple reaction by tyrosinase<sup>45</sup> (Figure 17). 2-Nap-Gly-Phe-Phe-Tyr (2Nap-GFFY) was used as the hydrogelator

precursor. The hydrogel was formed in the presence of various amounts of silica nanoparticles using the ENAC method (enzyme-assisted nanoparticle crosslinking). This method is inspired by the structure of marine mussel foot byssus, which is made of protein complexes with nano-sized granular structures through coordinate bonds mediated mainly by Dopa.

After the hydrogel is formed, a desired amount of mushroom tyrosinase is added to the hydrogel to convert the tyrosine residue into Dopa. This creates interactions between fibrils and silica nanoparticles. Because the crosslinking is introduced after the self-assembly of peptide fibrils, they could effectively minimize the interference between these two processes. Moreover, because of the crosslinks formed between Dopa and silica nanoparticles, the mechanical stability of the hydrogel was significantly enhanced.

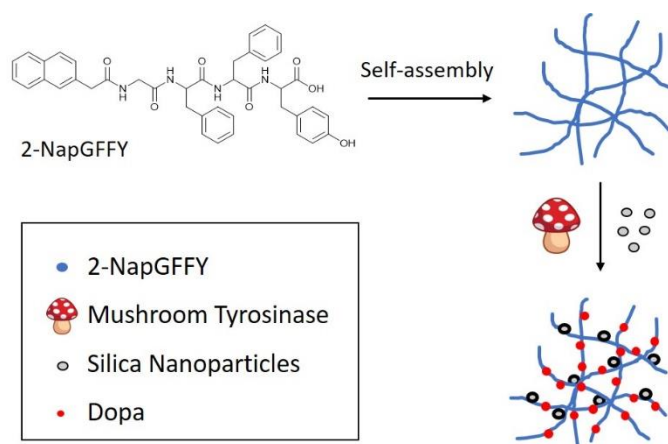


**Figure 17.** Schematic illustration of the ENAC strategy for hydrogelation of 2-NapGFFY.

Gazit *et al.* reported the synthesis and the assembly into fibrillar structures of Asp-Dopa-Asn-Lys-Dopa, that is a pentapeptide containing two Dopa units.<sup>46</sup> The peptide was dissolved in water and sonicated for 10 min, leading to a viscous turbid solution for all the concentration tested (100  $\mu$ M to 15 mM). TEM analyses revealed a network of fibrillar assemblies, mostly linear, unbranched and extending to the length of micrometers (Figure 18).

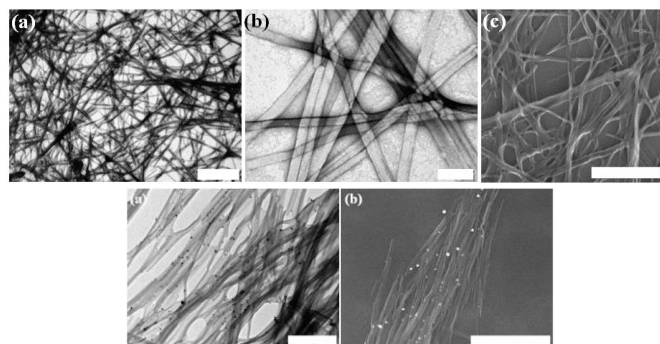


**Figure 18.** (Top) High-resolution microscopy of fibrillar assemblies formed by 6 mM Asp-Dopa-Asn-Lys-Dopa in water. (a,b) Transmission electron microscopy (TEM) micrographs, negative staining was applied; Scale bars represent 2  $\mu$ m and 100 nm; (c) scanning electron microscopy (SEM) micrograph, scale bar represents 1  $\mu$ m. (Bottom) Silver reduction by the Asp-Dopa-Asn-Lys-Dopa fibrillar assemblies. (a) TEM micrograph, negative staining was not applied. Scale bar represents 500 nm; (b) respective SEM micrograph, metallic coating by sputtering was not applied. Scale bar represents 2  $\mu$ m.

From the CD and FTIR analysis, it was suggested that Asp-Dopa-Asn-Lys-Dopa adopts either a random coil conformation or a  $\beta$ -turn conformation in water and that the  $\beta$ -turn structures self-assemble into supramolecular  $\beta$ -sheets, giving rise to amyloid-like fibrillar assemblies.

Finally, the authors tested the ability of the peptide to reduce ionic silver, that was confirmed by the appearance of dark nanometric clusters on the fibrillar assemblies, by both TEM and SEM. The clusters were not observed in a control solution to which  $\text{AgNO}_3$  was not added (Figure 20), while they seemed to have selectively deposited on the assemblies compared to the background. These results showed that Asp-Dopa-Asn-Lys-Dopa assemblies possess the ability to reduce ionic silver while retaining their ultrastructure in solution.

#### Self-assembled Longer Dopa-Containing Chains

Longer peptides, containing one or more Dopa units deserve some attention, as they exploit interesting properties.

Veldkamp *et al.* reported the incorporation of L-Dopa inside of a series of peptides designed to adopt a  $\beta$ -hairpin configuration (Figure 21). They demonstrated that these peptides including L-Dopa were able to form metal:peptide complexes with zinc.<sup>47</sup>

Absorption spectroscopy has proven to be a useful technique in studying metal-catecholic interactions. The formation of a ligand to metal charge transfer manifests as a novel absorbance. The combination of these DopaXxx peptides and zinc gives rise to a spectrophotometric change. While neither the L-Dopa containing peptides nor zinc solutions have significant absorbance above 300 nm, as DopaGly has only one aromatic ring with  $k_{\text{max}}$  at 283 nm. The titration of zinc yields an enhancement of the  $\pi$ - $\pi^*$  transition with red shifting. Notably, a new absorbance between 300 and 350 nm appears with increasing zinc (Figure 19). The absorbance that develops near 330 nm is consistent with changes to the L-Dopa aromatic ring upon metal binding.<sup>48</sup> Upon their mixing all investigated DopaXxx peptides develop similar absorbance bands

between 300–370 nm and experience a mild  $\pi$ - $\pi^*$  enhancement with modest changes to the  $k_{\max}$  between 278 and 283 nm.

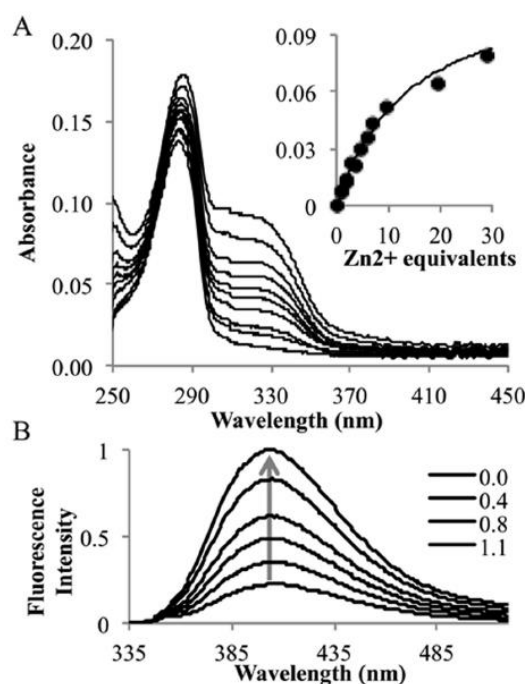


**Figure 19.** A) Spectrophotometric titration of DopaGly with Zn<sup>2+</sup>, insert shows the absorbance at 325 nm. B) Fluorescence emission with zinc addition from 0 to 1.4 equivalents. Adapted with permission from ref. 47. Copyright (2017) Elsevier.

Tang *et al.* reported the preparation of dendrimers (up to 30 residues) entirely made of L-Dopa (Figure 20).<sup>49</sup> Their monodisperse nature was shown by NMR, MALDI-TOF-MS, and PAGE. Individual L-Dopa moieties in the dendrimer were connected to one another via hydrolysable diester linkages. These Dopa dendrimers showed a 20-fold increase in aqueous solubility and enhanced photostability in solutions over L-Dopa under identical conditions.

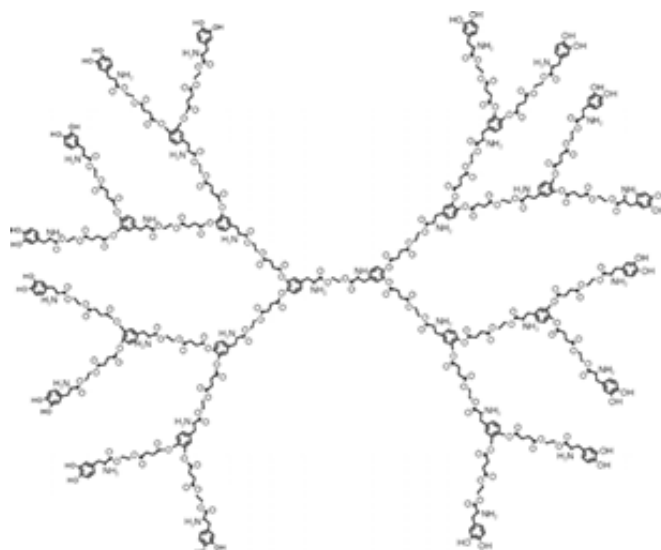


**Figure 20.** Structure of the second-generation L-DOPA dendrimer prodrug (HO-G2-NH<sub>2</sub>). Adapted with permission from ref. 49. Copyright (2006) American Chemical Society.

Li *et al.* reported the synthesis of a series of multidomain peptides (MDPs) able to self-assemble into nanofibres.<sup>50</sup> MDPs with the general sequence of K<sub>2</sub>(SLXL)<sub>3</sub>K<sub>2</sub> were prepared, where X was either serine, phenylalanine, tyrosine, or Dopa. When hydrogels were prepared by simple mixing of the Dopa-substituted MDP (K<sub>2</sub>(SLZL)<sub>3</sub>K<sub>2</sub>) with Hank's Buffered Salt Solution (HBSS), the properties of the obtained material were similar to the unsubstituted peptide (K<sub>2</sub>(SL)<sub>6</sub>K<sub>2</sub>). They then examined the possibility to induce a shear alignment of the nanofibers. K<sub>2</sub>(SLZL)<sub>3</sub>K<sub>2</sub> was prepared in a gel-loading tip and slowly injected into the HBSS buffer solution while dragging the pipet backward. They observed the formation of a string of hydrogel with unique mechanical strength, easily lifted by tweezers without breaking. Examination of the string by polarized optical microscopy revealed strong birefringence along the length of the fibers, suggesting the anisotropic nature of the string, in agreement with SEM and TEM analyses, which revealed the presence of bundles of aligned nanofibers. These mechanical strength and morphology were not found in K<sub>2</sub>(SL)<sub>6</sub>K<sub>2</sub> (the non-containing Dopa analogue) prepared in the same way (Figure 21). Since this difference in long-range organization could have been ascribed to the aromatic side chain of Dopa, they also prepared two additional MDPs, K<sub>2</sub>(SLFL)<sub>3</sub>K<sub>2</sub> and K<sub>2</sub>(SLYL)<sub>3</sub>K<sub>2</sub>, replacing Dopa with phenylalanine (F), bearing a benzyl ring but no hydroxylation, and tyrosine (Y) bearing a benzyl ring with one hydroxyl group.

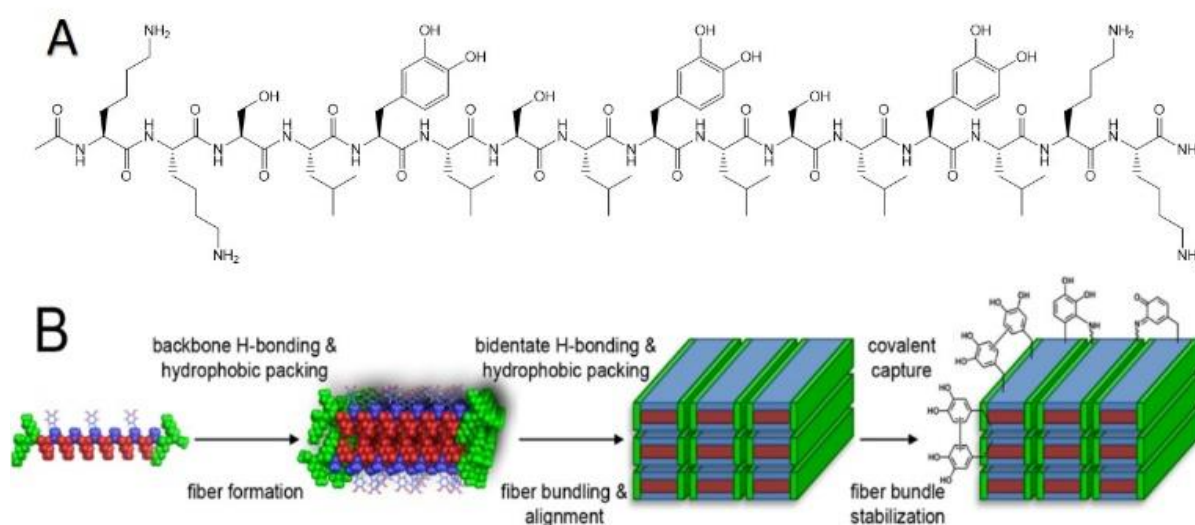
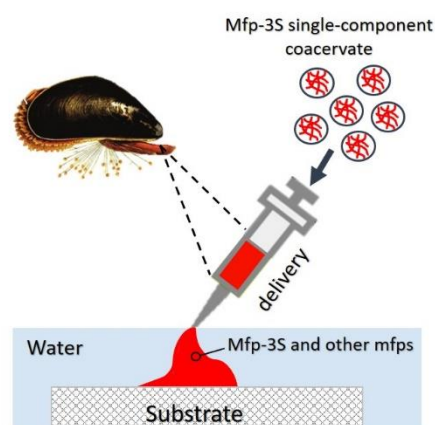


**Figure 21.** Schematic of multidomain peptides forming aligned self-assembling nanofibers. (A) Chemical structure of Dopa-containing MDP sequence  $K_2(SLZL)_3K_2$ . (B) Process of self-assembly, fiber bundling, fiber alignment, and covalent capture. The inclusion of Dopa introduces hydrophobic moieties in addition to the potential for bidentate hydrogen bonding on the surface to reinforce the observed parallel packing of fibers. Upon oxidation, these groups can covalently cross-link with one another or with the amines of the lysine residues.

When they prepared the gel inducing the shear alignment, strings were formed in both cases but did not show birefringence, which was similar to  $K_2(SL)_6K_2$ . Also, these strings were not strong enough to be lifted from solution or otherwise manipulated after creation, but easily fragmented instead, highlighting the role of Dopa in the structure.

They also oxidised Dopa with periodate to initiate covalent cross-linking. They obtained strings mechanically strong enough to be manipulated and chemically resilient enough to survive transfer into media, which, without the covalent cross-links, would result in peptide disassembly.

Wei *et al.* designed a peptide analogue of mfp3 (mfp3S-pep), comprised of 25 amino acids to mimic the native protein (Figure 22).<sup>51</sup> Using mushroom tyrosinase the peptide was enzymatically modified to provide the desired level of Tyr to Dopa conversion (mfp3S-pep-Dopa). The self-coacervation of the modified and unmodified peptides was investigated over a range of pH and ionic strength. Hydroxyapatite (HAP) and  $TiO_2$  (anatase) surfaces were used for adsorption studies for their relevance in biomedical applications. Adsorption studies performed on HAP and  $TiO_2$  confirmed that Dopa promotes faster initial adsorption kinetics, with the coacervate highly enhancing the quantity of adsorbed peptide.



<b>representative variant of mfps-3S:</b>	
GYGYDLGYNAPWPYNNNGYGYNGYHGRYGNKGWNNNGPWGGY	
<b>Mfps3S-pep:</b>	
GY	D GYN WPY GY NGY RYGNKGW N GY
<b>Mfp-3S</b>	45 aa, pl: 7-8
<b>Mfps3S-pep</b>	25 aa, pl: 8.3

**Figure 22.** Mussel derived phase-separating adhesive proteins and their peptide mimics. Upper: schematic illustration of mfp-3S being delivered onto a wet substrate surface in the form of a single-component coacervate followed by its hardening into the mussel's adhesive plaque together with other mfps. Lower: sequences of native mfp-3S and truncated peptide mfp3S-pep with their corresponding pl. Letters in red, blue, and green denote aromatic, basic, and acidic amino acids, respectively.

Finally, Xu *et al.* studied the dimension of the nanostructures self-assembled from short designed peptides, analysing the behaviour of peptide bolaamphiphiles (Figure 23).<sup>52</sup> These molecules form monolayer wall nanotubes, facilitated by the interplay between the



side chain structure and hydrophobicity of the central residues. The peptide  $KI_4K$  self-assembles into nanotubes with a width of  $\sim 100$  nm. The three variants of  $KI_4K$ , via the substitution of aromatic amino acids (F, Y, and Dopa) for the I residue closest to the C-terminus, reduces the nanotube diameters, indicating a significant steric hindrance of the benzene rings on the lateral packing of  $\beta$ -sheets. However, the introduction of hydroxyl groups on the benzene rings alleviates the steric effect, with nanotube diameter increasing in the order of  $KI_3FK$ ,  $KI_3YK$ , and  $KI_3DopaK$ . With increasing incubation time, monolayered twisted ribbons and helical ribbons grow into mature  $KI_3DopaK$  nanotubes via the pitch closing route.

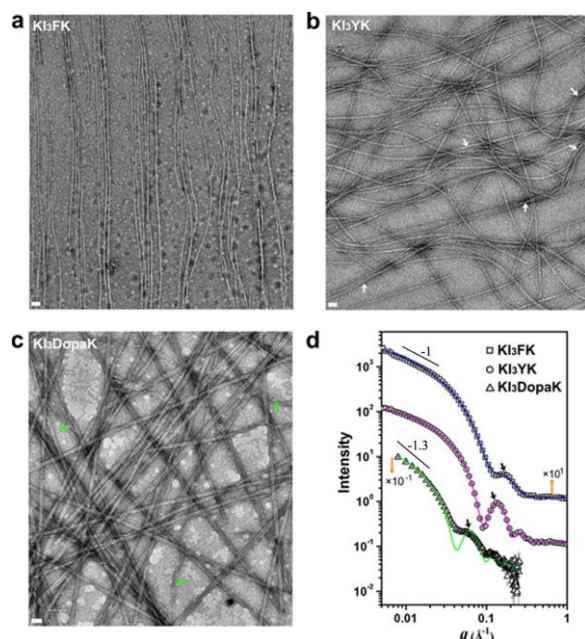


**Figure 23.** Structural characterizations of the self-assemblies formed by the designed bolapeptides in water (32 mM) after 1 week of incubation. (a-c) negative-staining TEM images (scale bar, 50 nm). White arrows in b indicate further aggregation of thin  $KI_3YK$  assemblies, and green arrows in c show the presence of minor helical ribbons, as the precursor of the dominant nanotubes. (d) SANS data and model fits. Adapted with permission from ref. 52. Copyright (2021) Elsevier.

## Surface Coatings with L-Dopa: Layers and Self-Assembled Nanospheres

The last chapter of this review is dedicated to Dopa containing peptides that do not form materials themselves, but act as surface coatings, thus modifying the properties of the material that is treated with these peptides. We include here also the use of Dopa peptoids, that mimic peptides as they are chains having an achiral  $\alpha$ -carbon, while the chiral moiety is linked to the nitrogen.

Chen *et al.* reported the preparation of Dopa adlayers on self-assembled monolayers (SAMs) with varying end groups ( $-OH$ ,  $-NH_2$  and  $-CF_3$ ).<sup>53</sup> The bare surface tested was gold (Figure 24a).

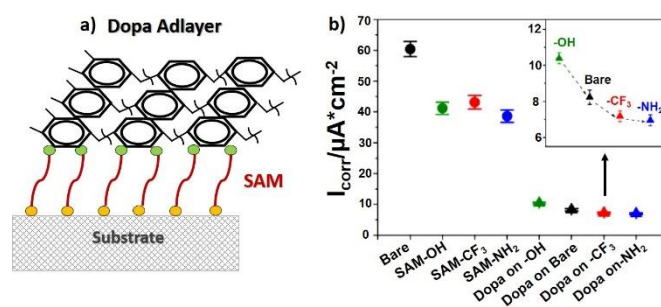


**Figure 24.** (a) Formation of Dopa adlayers; (b) Corrosion current obtained from potentiodynamic polarization curves for different Dopa adlayers

The well-defined and highly ordered monolayers and the compact L-Dopa adlayers protect the substrate from corrosion, suppressing the diffusion of aggressive water and acid molecules. The authors found that corrosion current ( $I_{corr}$ ) decreases with the introduction of Dopa adlayers on  $-CF_3$  and  $-NH_2$  SAMs but increases with the addition of Dopa on  $-OH$  SAMs, compared with Dopa adlayers coating on bare substrate (Figure 24b).

The authors correlated the corrosion resistance with the binding energy and with the molecular orientation. The binding energy values of Dopa upon OH-SAMs indicates an “upright” conformation with the carboxyl orienting perpendicularly toward the surface and a formation of hydrogen bond between Dopa and OH-SAMs (Figure 25 a). In the case of bare substrate, there are both “flat” and “upright” conformations with the phenylene ring plane lying parallel to the surface or hydroxyls group of the catechol orienting perpendicularly toward the surface, leading to a relative loose and extended adlayer (Figure 25 b). The values of Dopa interacting with  $-NH_2$  and  $-CF_3$  SAMs suggested a “flat” conformation on both surfaces (Figure 25 c).

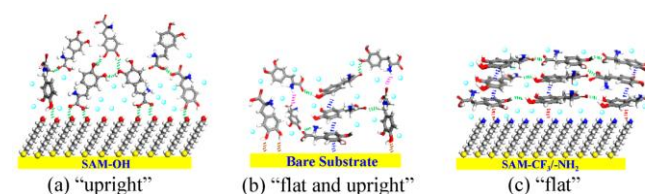


**Figure 25.** Optimized preferential adsorption conformations of Dopa on (a) OH-SAMs, (b) bare substrate, (c)  $CF_3$ - and  $NH_2$ - SAMs. Adapted with permission from ref. 53. Copyright (2019) Elsevier.

Another application is described by Messersmith *et al.*, who studied the adhesion of peptides of various length with repeating unit Lys-Dopa (KZ) and Lys-Phe (KF) with polystyrene (PS) and  $TiO_2$  (Figure 26).<sup>54</sup>

Comparing (Lys-Dopa), (Lys-Dopa)<sub>3</sub>, (Lys-Dopa)<sub>10</sub>, the authors found that the adhesion toward TiO<sub>2</sub> is increased from the monomer (SMFS, 120 pN) to the trimer (SMFS, 300 pN), but this remains steady for higher number of repeating units. TiO<sub>2</sub> surface is negatively charged, so it is reasonable that a major number of Lys residues results in an increase of the adhesion ability. Also, an increase in the positive charge results in a better removal of the water layer from the surface to bind. In the end, in (KZ)<sub>3</sub> the repetitive sequence allows the formation of the symmetric feature Lys-Dopa-Lys, leading to a more adaptable and versatile synergistic binding.

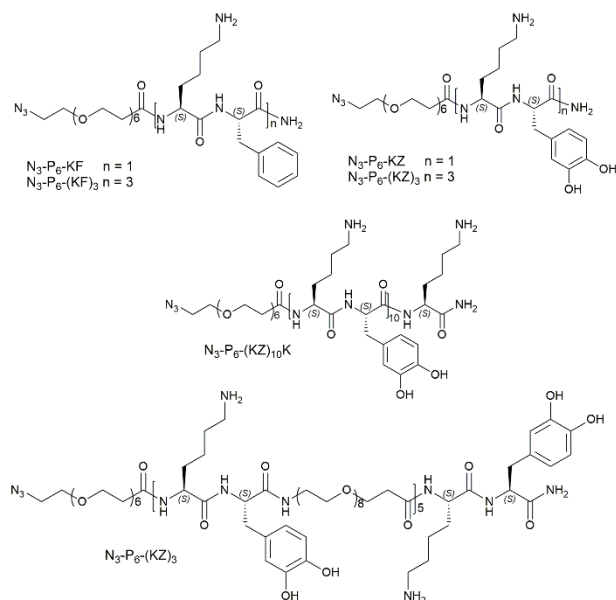


**Figure 26.** Chemical structure of the synthesized peptides.

To investigate how the substitution of Dopa with Phe would affect the adhesion capability, the same oligomers, in terms of peptide length, were synthesised, (Lys-Phe), (Lys-Phe)<sub>3</sub> and (Lys-Phe)<sub>10</sub> and deposited on TiO<sub>2</sub> and polystyrene. (Lys-Phe) oligomers show remarkable adhesion capability toward polystyrene, while being slightly adhesive with TiO<sub>2</sub>. This may be explained considering the fact that Phe interacts with the surface through cation- $\pi$  and  $\pi$ - $\pi$  interactions: a PS surface is easily bound by such molecules, while a negatively charged one is less likely to be bound, resulting in a non-detectable force for the dipeptide and a remarkably lower one for superior oligopeptides.

In another work on coating with peptides, Reches *et al.* reported a tripeptide sequence containing three elements that enable (i) self-assembly into a coating, (ii) adsorption onto any substrate and (iii) antifouling activity. To direct the assembly of the peptide, they selected two adjacent fluorinated phenylalanine residues.<sup>55</sup> They assumed that due to aromatic interactions this motif promotes molecular recognition and directs the self-assembly of the peptide into a film. In addition, the carbon-fluorine bond of the fluorinated aromatic ring would lead to the formation of a "Teflon-like" material that will prevent the attachment of proteins to the surface and therefore will act as antifouling motif. The insertion of L-Dopa into the peptide sequence would act as a glue and immobilizes the peptide on different substrates (Figure 27). They compared four peptides: Dopa-Phe(4F)-Phe(4F), Dopa-Phe(F<sub>5</sub>)-Phe(F<sub>5</sub>), Dopa-Phe-

Phe and Dopa-Phe(F<sub>4</sub>). Overall, these results demonstrate that, in order to achieve antifouling activity, the peptide must contain fluorinated phenylalanine residues, which avoids the adsorption of proteins on the coated surface. The best antifouling activity was achieved with Dopa-Phe(4F)-Phe(4F).

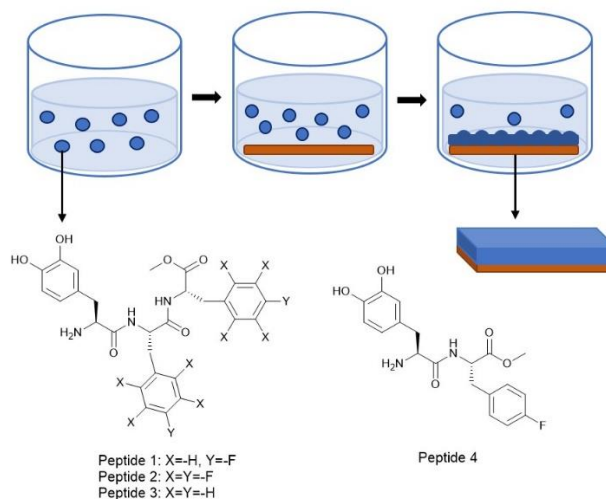


**Figure 27.** The illustration in the upper panel shows the formation of a coating on a substrate by dip coating. The lower panel illustrates the molecular structures of the studied peptides.

The same group explored three variations of Dopa-Phe(4F)-Phe(4F), each with a different end group (Figure 28).<sup>56</sup> This study shows that different groups at the C-terminus can lead to a change in the peptide assembly on titanium surface and its adsorption process.

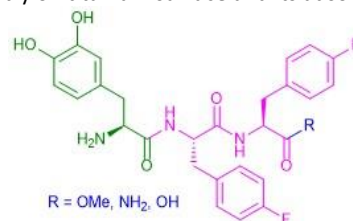


**Figure 28.** The chemical structure of the peptides of R-COOMe, R-CONH<sub>2</sub>, and R-COOH. Dopa is in green, the antifouling motif, fluorinated phenylalanine, in pink, and the different ending groups, in blue.

Peptide R-COOH had the highest adsorption, R-CONH<sub>2</sub> medium, and R-COOMe the smallest adsorption, that also corresponds to an increase in the thickness of the adsorbed layer.

The surfaces were incubated with Gram-negative and Gram-positive bacteria, to assess the bacterial attachment to the surface. There was no significant difference between the peptides for the reduction of *E. coli*, while, with *S. epidermidis*, the antifouling effect was lower than with Gram positive bacteria. This difference in bacterial adhesion (Gram positive versus Gram negative) might be due to the variation in surface energy.



L-Dopa was also used to mediate the immobilization of bioactive nanofibers on titanium surface in the presence of water through catechol–titanium coordination. Ceylan *et al.* synthesized a peptide amphiphile (PA) molecule covalently conjugated to Dopa (Lauryl-VVAGE-Dopa-Am, Dopa-PA) for titanium surface functionalization and another PA molecule conjugated to a heparin-binding adhesion peptide sequence, KRSR (Lauryl-VVAGKRSR-Am, KRSR-PA) to promote osteogenic activity (Figure 29).<sup>57</sup> Neither Dopa-PA nor KRSR-PA formed an organized structure by themselves in solution at

pH 7.4. However, upon mixing, they predominantly formed  $\beta$ -sheet structures within seconds, indicating  $\beta$ -sheet-driven nanofibers formation. The rheological analysis confirmed the formation of a weak gel with  $G'$  around 40 Pa.

The binding of the KRSR-PA/Dopa-PA nanofibers on the titanium surface was then investigated in the presence of water using X-ray photoelectron spectroscopy (XPS) after a rinsing step on the surface. They confirmed the permanent adsorption of KRSR-PA/Dopa-PA nanofibers and the formation of a peptide surface coating.

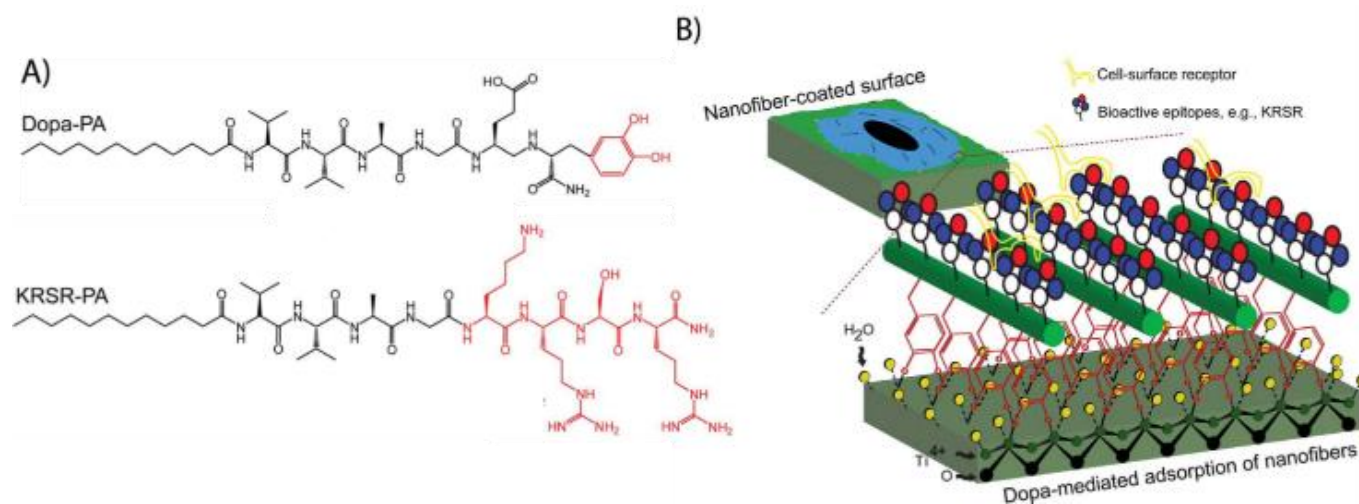


**Figure 29.** (A) Chemical structures of the peptide amphiphile molecules designed for functionalization of titanium surfaces. (B) Dopa-mediated immobilization of the bioactive nanofibers on titanium surface in the presence of water is shown to occur through catechol–titanium coordination.<sup>58</sup> Adapted with permission from ref. 57. Copyright (2012) Royal Society of Chemistry.

The authors reported also that osteoblastic Saos2 cells adhered in significantly greater numbers on KRSR-PA/Dopa-PA compared to the bare  $\text{TiO}_2$  surface. The increased hydrophilicity of the decorated surface also caused a decrease in the number of human gingival fibroblasts (HGF) adhered on the surface, this resulting in the designed PA coatings to selectively favour osteoblast adhesion. Saos2 cell viability also gained a selective enhancement on KRSR-PA/Dopa-PA coatings.

#### Surface Coatings with L-Dopa Peptoids

The adhesive performances of MFPS (mussels foot proteins) are largely due to cohesive effects. The catecholic (Dopa) and cationic (Lys, Arg) side chains work separately and in synergy to maximize both adhesion and cohesion in mfps.

Comparing Phe-, Tyr- and Dopa-peptides, Phe have the strongest cohesive forces. Cation- $\pi$  interactions are the main responsible of cohesion, which is limited by the steric hindrance of hydroxyl groups in the case of Tyr and Dopa.

Opposite results have been obtained by Waite *et al.* with peptoids, that are chains having an achiral  $\alpha$ -carbon, no amide hydrogens (which prevents the formation of H bond) and poor electron delocalization in the polyamide backbone bonds, leading to a more flexible conformation (Figure 30).<sup>59</sup>

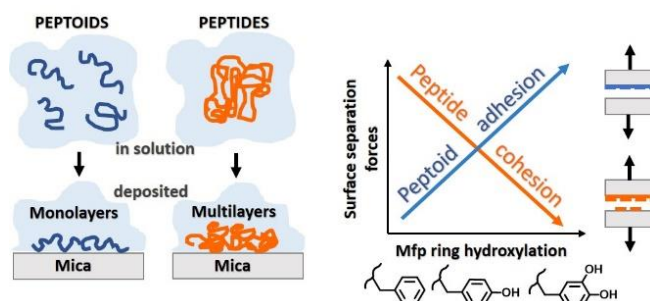


**Figure 30.** Illustration of the assembly of peptoids and peptides in solution and after deposition (left). Surface separation forces in peptides and peptoids depending on the ring hydroxylation (right).

Thanks to the flexibility of their backbones, peptoids tend to deposit as a monomolecular film, while peptides deposit as multilayers and this induces an opposite trend between them. Peptoids are more hydrophobic and therefore less hydrated than Dopa-containing peptides, so the surface and molecular binding properties are largely dominated by H-bonding and cation- $\pi$  interactions. Thus, for peptides the trend in adhesion (and cohesion) is Phe > Tyr > Dopa, and for peptoids we have the opposite trend. Peptoids may be used as substitutes for peptides, maintaining the properties of the side chains, yet avoiding the complications due to the rigidity of the backbone (Figure 31).

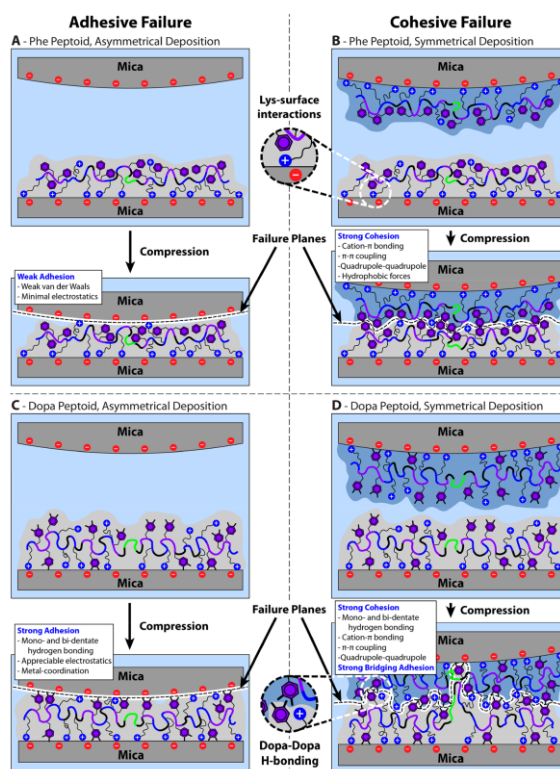


**Figure 31.** Modeling peptoid adhesion vs cohesion. Scheme of peptoid films before and after compression for asymmetric deposition of the Phe peptoid (A), symmetric deposition of the Phe peptoid (B), asymmetric deposition of the Dopa peptoid (C), and symmetric deposition of the Dopa peptoid (D). Adapted with permission from ref. 59. Copyright (2020) American Chemical Society.

## Conclusions

Protected Dopa and peptides containing Dopa form a group of molecules able to self-assemble into a plethora of materials holding remarkable properties ranging from gels to adhesives and nanoparticles. These peptides may also functionalize materials surfaces, to modify their properties.

The capability of Dopa to form supramolecular materials is due to the presence of multiple interacting sites present on it, that make it a multifunctional building block. The possibility to form hydrogen bonds and the presence of the aromatic ring allow L-Dopa molecules to interact through a series of non-covalent interactions. The additional presence of the catechol moiety has implications in the self-assembly process of Dopa itself and with other substrates.

In this review we have collected a wide variety of examples, that have been classified according to the peptide size. It is remarkable to see that even protected Dopa can form several different materials, simply changing the protecting groups, the solvent and the trigger. The versatility of more complex peptides is even higher. We hope that this review will spur the community of chemists to make further efforts in the study of Dopa based materials.

## Author Contributions

Conceptualization: DG and CT; Funding acquisition: CT; Investigation: DG and PR; Writing – original draft: DG, PR and CT; Writing – review & editing: DG, PR and CT.

## Conflicts of interest

There are no conflicts to declare.

## Notes and references

- 1 D. A. Robb, *Tyrosinase*, CRC Press, 2018.
- 2 M. T. Varela, M. Ferrarini, V. G. Mercaldi, B. da S. Sufi, G. Padovani, L. I. S. Nazato and J. P. S. Fernandes, *Bioorg. Chem.*, 2020, **103**, 104108.
- 3 K. Min, D. H. Park and Y. J. Yoo, *J. Biotechnol.*, 2010, **146**, 40–44.
- 4 E. Waser and M. Lewandowski, *Helv. Chim. Acta*, 1921, **4**, 657–666.
- 5 T. Shimidzu, T. Iyoda and N. Kanda, *J. Chem. Soc. Chem. Commun.*, 1981, 1206–1207.
- 6 T. Ooi, M. Kameda, H. Tannai and K. Maruoka, *Tetrahedron Lett.*, 2000, **41**, 8339–8342.
- 7 I. A. Sayyed and A. Sudalai, *Tetrahedron Asymmetry*, 2004, **15**, 3111–3116.
- 8 R. H. Valdés, L. Puzer, M. Gomes, C. E. S. J. Marques, D. A. G. Aranda, M. L. Bastos, A. L. Gemal and O. A. C. Antunes, *Catal. Commun.*, 2004, **5**, 631–634.
- 9 D. Magdziak, A. A. Rodriguez, R. W. Van De Water and T. R. Pettus, *Org. Lett.*, 2002, **4**, 285–288.
- 10 R. Bernini, M. Barontini, F. Crisante, M. C. Ginnasi and R. Saladino, *Tetrahedron Lett.*, 2009, **50**, 6519–6521.
- 11 M. D'Ischia, A. Napolitano, V. Ball, C. T. Chen and M. J. Buehler, *Acc. Chem. Res.*, 2014, **47**, 3541–3550.
- 12 J. H. Waite, *Int. J. Adhes. Adhes.*, 1987, **7**, 9–14.
- 13 S. A. Mian and Y. Khan, *J. Chem.*, 2017, **2017**, 1–6.
- 14 J. H. Waite, *J. Exp. Biol.*, 2017, **220**, 517–530.
- 15 S. Barbara, *Biochemistry*, 2002, **1180**, 1172–1180.
- 16 J. H. Waite and M. L. Tanzer, *Top. Catal.*, 1980, **96**, 1554–1561.
- 17 B. P. Lee, P. B. Messersmith, J. N. Israelachvili and J. H. Waite, *Annu. Rev. Mater. Res.*, 2011, **41**, 99–132.
- 18 H. Zhao, C. Sun, R. J. Stewart and J. H. Waite, *J. Biol. Chem.*, 2005, **280**, 42938–42944.
- 19 J. H. Waite, *Integr. Comp. Biol.*, 2002, **42**, 1172–1180.
- 20 W. Zhang, R. Wang, Z. M. Sun, X. Zhu, Q. Zhao, T. Zhang, A. Cholewinski, F. Yang, B. Zhao, R. Pinnaratip, P. K. Forooshani and B. P. Lee, *Chem. Soc. Rev.*, 2020, **49**, 433–464.
- 21 N. Pandey, L. F. Soto-Garcia, J. Liao, P. Zimmern, K. T. Nguyen and Y. Hong, *Biomater. Sci.*, 2020, **8**, 1240–1255.
- 22 W. Y. Quan, Z. Hu, H. Z. Liu, Q. Q. Ouyang, D. Y. Zhang, S. D. Li, P. W. Li and Z. M. Yang, *Molecules*, 2019, **24**, 1–27.
- 23 L. Li, W. Smitthipong and H. Zeng, *Polym. Chem.*, 2015, **6**, 353–358.
- 24 Q. Guo, J. Chen, J. Wang, H. Zeng and J. Yu, *Nanoscale*,

- 2020, **12**, 1307–1324.
- 25 P. Kord Forooshani and B. P. Lee, *J. Polym. Sci. Part A Polym. Chem.*, 2017, **55**, 9–33.
- 26 I. Manolakis and U. Azhar, *Coatings*, 2020, **10**.
- 27 B. K. Ahn, S. Das, R. Linstadt, Y. Kaufman, N. R. Martinez-Rodriguez, R. Mirshafian, E. Kesselman, Y. Talmon, B. H. Lipshutz, J. N. Israelachvili and J. H. Waite, *Nat. Commun.*, 2015, **6**, 1–7.
- 28 H. T. Peng and P. N. Shek, *Expert Rev. Med. Devices*, 2010, **7**, 639–659.
- 29 M. De Loos, B. L. Feringa and J. H. Van Esch, *European J. Org. Chem.*, 2005, 3615–3631.
- 30 J. Wang, K. Liu, R. Xing and X. Yan, *Chem. Soc. Rev.*, 2016, **45**, 5589–5604.
- 31 E. R. Draper and D. J. Adams, *Chem*, 2017, **3**, 390.
- 32 X. Du, J. Zhou, J. Shi and B. Xu, *Chem. Rev.*, 2015, **115**, 13165–13307.
- 33 C. Tomasini and N. Castellucci, *Chem. Soc. Rev.*, 2013, **42**, 156–172.
- 34 A. Saha, S. Bolisetty, S. Handschin and R. Mezzenga, *Soft Matter*, 2013, **9**, 10239.
- 35 G. Fichman, T. Guterman, J. Damron, L. Adler-Abramovich, J. Schmidt, E. Kesselman, L. J. W. Shimon, A. Ramamoorthy, Y. Talmon and E. Gazit, *Sci. Adv.*, 2016, **2**, 1–11.
- 36 K. A. Houton, K. L. Morris, L. Chen, M. Schmidtman, J. T. A. Jones, L. C. Serpell, G. O. Lloyd and D. J. Adams, *Langmuir*, 2012, **28**, 9797–9806.
- 37 G. Fichman, T. Guterman, L. Adler-abramovich and E. Gazit, *CrystEngComm*, 2015, **17**, 8105–8112.
- 38 D. Giuri, L. Jurković, S. Fermani, D. Kralj, G. Falini and C. Tomasini, *ACS Appl. Bio Mater.*, 2019, **2**, 5819–5828.
- 39 C. Lee, S. H. Kim, J. H. Jang and S. Y. Lee, *Sci. Rep.*, 2017, **7**, 1–11.
- 40 D. Giuri, K. A. Jacob, P. Ravarino and C. Tomasini, 2020, 1–8.
- 41 N. Zanna, D. Iaculli and C. Tomasini, *Org. Biomol. Chem.*, 2017, **15**, 5797–5804.
- 42 C. Tomasini and N. Zanna, *Biopolymers*, 2017, **108**, 1–14.
- 43 D. Giuri, N. Zanna and C. Tomasini, *Gels*, 2019, **5**, 27.
- 44 G. Fichman, L. Adler-Abramovich, S. Manohar, I. Mironi-Harpaz, T. Guterman, D. Seliktar, P. B. Messersmith and E. Gazit, *ACS Nano*, 2014, **8**, 7220–7228.
- 45 Y. Li, M. Qin, Y. Cao and W. Wang, *Sci. China Physics, Mech. Astron.*, 2014, **57**, 849–858.
- 46 G. Fichman, T. Guterman, L. Adler-Abramovich and E. Gazit, *Nanomaterials*, 2014, **4**, 726–740.
- 47 K. L. Veldkamp, P. J. Tubergen, M. A. Swartz, J. T. DeVries and C. D. Tatko, *Inorganica Chim. Acta*, 2017, **461**, 120–126.
- 48 M. R. Eftink, L. R. A. Selvidge, P. R. Callis and A. A. Rehms, *J. Phys. Chem.*, 1990, **94**, 3469–3479.
- 49 S. Tang, L. J. Martinez, A. Sharma and M. Chai, *Org. Lett.*, 2006, **8**, 4421–4424.
- 50 I. C. Li and J. D. Hartgerink, *J. Am. Chem. Soc.*, 2017, **139**, 8044–8050.
- 51 W. Wei, L. Petrone, Y. Tan, H. Cai, J. N. Israelachvili, A. Miserez and J. H. Waite, *Adv. Funct. Mater.*, 2016, **26**, 3496–3507.
- 52 Y. Zhao, X. Hu, L. Zhang, D. Wang, S. M. King, S. E. Rogers, J. Wang, J. R. Lu and H. Xu, *J. Colloid Interface Sci.*, 2021, **583**, 553–562.
- 53 T. Chen, M. Yang, H. Yang, R. Wang, S. Wang, H. Zhang, X. Zhang, Z. Zhao and J. Wang, *J. Ind. Eng. Chem.*, 2019, **69**, 179–186.
- 54 Y. Li, J. Cheng, P. Delparastan, H. Wang, S. J. Sigg, K. G. DeFrates, Y. Cao and P. B. Messersmith, *Nat. Commun.*, 2020, **11**, 1–8.
- 55 S. Maity, S. Nir, T. Zada and M. Reches, *Chem. Commun.*, 2014, **50**, 11154–11157.
- 56 A. Dolid and M. Reches, *J. Pept. Sci.*, , DOI:10.1002/psc.3212.
- 57 H. Ceylan, S. Kocabey, A. B. Tekinay and M. O. Guler, *Soft Matter*, 2012, **8**, 3929–3937.
- 58 T. H. Anderson, J. Yu, A. Estrada, M. U. Hammer, J. H. Waite and J. N. Israelachvili, *Adv. Funct. Mater.*, 2010, **20**, 4196–4205.
- 59 W. R. Wonderly, T. R. Cristiani, K. C. Cunha, G. D. Degen, J. E. Shea and J. H. Waite, *Macromolecules*, 2020, **53**, 6767–6779.